VII. SIMULATION OF SOLAR-WIND - EARTH-MAGNETOSPHERE INTERACTION

Donald L. Chubb

Research on solar-wind - Earth-magnetosphere interaction at the Lewis Research Center was a natural outgrowth of research on magnetoplasmadynamic (MPD) arc thrusters. These thrusters were discussed in the paper by Seikel et al. Figure VII-1 shows the flow obtained in the initial exploratory experiments. The highly ionized high-velocity hydrogen exhaust of the water-cooled MPD arc on the right is used to represent the solar-wind flow. A dipole electromagnet in the insulated globe simulates the Earth's magnetic field.

Although these preliminary experiments were encouraging, significant improvements are required to obtain an adequate simulation of solar-wind - Earth-magnetosphere interaction. This paper describes the progress being made toward that goal.

CHARACTERISTICS OF SOLAR-WIND - EARTH-MAGNETOSPHERE INTERACTION

A complete discussion of the solar-wind - Earth-magnetosphere interaction is given by Hess (ref. 1). Figure VII-2 shows the pertinent details of the interaction. The solar wind, which has a density of ~3 particles per cubic centimeter, is made up of electrons, protons, and some helium nuclei and is therefore a plasma. It flows radially from the Sun with a velocity of $\sim 4\times10^5$ meters per second and a temperature of $\sim 10^5$ K. Imbedded in this plasma flow is a magnetic field of $\sim 4\times10^{-9}$ tesla that originates at the Sun. It should be emphasized that these solar-wind properties increase by factors of 2 or 3 during periods of solar activity. The properties of the wind are such that the flow is supersonic. (For a plasma flow to be supersonic, the square of the velocity must be greater than the sum of the squares of the sound speed and the Alfven speed.) Therefore, just as in the case of an aircraft flying supersonically in the atmosphere, a shock wave forms when the

solar wind impinges on the Earth's magnetic field. The Earth's magnetic field acts like a solid body deflecting the solar-wind flow. The shock wave is about $13R_E$ from the Earth (R_E = Earth radius = 6.37×10^6 m) on the line connecting the Earth and Sun and has a thickness of $\sim 0.001R_E$. One of the most interesting details about this bow shock wave is that it is "collisionless," which means that the average distance a particle travels before colliding with another particle (mean free path) is large compared to some characteristic dimension. For the bow shock, the characteristic dimension is the thickness of the shock. In a conventional gas dynamic shock wave, it is the dissipation that results from particle collisions that accounts for the shock structure. However, for a plasma collisionless shock wave, it is the interaction of the charged particles and the electric and magnetic fields in the plasma that produces the dissipation.

As a result of passing through the shock wave, the solar wind is decelerated and compressed. The embedded magnetic field is also compressed. After passing through the shock the flow enters a region called the magnetosheath where the plasma properties show rapid fluctuations. Forming the boundary between the magnetosheath and the region where the Earth's magnetic field is confined is the magnetopause. The region where the Earth's magnetic field is confined is called the magnetosphere. Within the magnetopause electrical currents must flow in order to allow the transistion between the solar-wind magnetic field and the Earth's magnetic field. In figure VII-2 the solar-wind magnetic field and the Earth's magnetic field are not shown connected. Whether the magnetic field lines join or do not join is a question that has not been resolved as yet. If the field lines do connect, the magnetosphere is called open; if they do not connect, the magnetosphere is called closed. Figure VII-2 also shows the solar magnetic field at some angle to the solar-wind flow. This angle changes as the Earth rotates about the Sun.

Within the magnetosphere are the belts of trapped high energy electrons and protons usually called the Van Allen belts. These charged particles spiral about the Earth's magnetic field lines and are reflected back and forth between the North and South Poles. The radiation belts begin at about $1.5R_E$ and extend to about $8R_E$. From $1.5R_E$ to $2R_E$ many protons have energies greater than 30 MeV. This is usually called the inner radiation belt. In the region $3R_E$ to $4.5R_E$, which is called the outer belt, many electrons have energies greater than 1.6 MeV.

Trailing behind the Earth is the region called the geomagnetic tail. This tail is caused by the solar wind dragging the Earth's magnetic field along with it. Figure VII-2 shows the tail only out to $40R_E$. It is actually much longer and has been observed at distances beyond the Moon ($60R_E$). Within the geomagnetic tail is a region, called the neutral sheet, where the magnetic field is nearly zero. The

magnetic field changes direction across the neutral sheet. Associated with the geomagnetic tail is a band of keV energy charged particles denoted in figure VII-1 as the plasma sheet, which has a thickness of about $10R_E$.

SIMULATION CRITERIA

Now that a brief description has been given of the main features of the solar-wind - Earth interaction, a way to simulate the entire interaction in the laboratory is considered. The following discussion was first presented in reference 2. First of all, there must be a theoretical understanding of the phenomenon in order to know what conditions must be satisfied for its simulation. In the case of the solar-wind - Earth interaction there are very few completely accepted explanations for the various features of the interaction. Therefore, simulation is dependent on the criteria considered most important. We assume the following conditions (see fig. VII-3) must be satisfied for a proper simulation:

(1) Collisionless flow, $\lambda > \ell$

(2) Hypersonic flow, $M_s^2 >> 1$, $M_a^2 >> 1$

(3) Bow shock thin compared to standoff distance, $\delta < \Delta$

(4) Geometrical similarity, $a = 10R$

(5) Plasma beam diameter greater than interaction size, $d > 4a$

The terms introduced in these expressions are defined as follows: collisional mean free paths, λ; characteristic dimension of the experiment, ℓ; shock thickness, δ; shock standoff distance, Δ; distance from the center of the dipole to the edge of the magnetosphere, a; diameter of the dipole, R; diameter of the plasma beam, d; acoustic Mach number, M_s; and Alfven number, M_a.

In the following discussion each one of these conditions is considered. The simulation criteria resulting from these conditions are written in terms of the velocity u_1, the number density n_1 upstream of the shock, and the parameter a.

HYPERSONIC FLOW AND SHOCK CRITERIA

From satellite data it is known that both M_s and M_a are about 8. The acoustic Mach number is defined as

$$M_s^2 \equiv \frac{u_1^2}{C_1^2} \tag{1}$$

where

$$C_1^2 = \frac{5}{3}\frac{kT_1}{m_i} \tag{2}$$

is the upstream acoustic speed. The Alfven number M_a is defined as

$$M_a^2 \equiv \frac{u_1^2}{V_{a_1}^2} \tag{3}$$

where

$$V_{a_1}^2 = \frac{B_1^2}{m_i n_1 \mu_0} \tag{4}$$

is the upstream Alfven number. Other terms appearing in equations (1) to (4) are the velocity u_1, the temperature T_1, the magnetic field B_1, the number density n_1, the Boltzmann constant k, the ion mass m_i, and the magnetic permeability μ_0 (= 1.2556×10^{-6} H/m). The subscript 1 refers to conditions upstream of the shock (fig. VII-3).

The Mach number of the flow is defined as (ref. 8)

$$M_1^2 \equiv \frac{u_1^2}{C_1^2 + V_{a_1}^2} \equiv \frac{M_a^2 M_s^2}{M_a^2 + M_s^2} \tag{5}$$

Since M_a and M_s are both approximately 8, equation (5) yields $M_1 \approx 6$. In a simulation experiment it is difficult to achieve such large Mach numbers. However, to a first approximation the flow is required to be hypersonic. For hypersonic flow, $M_s^2 >> 1$ and $M_a^2 >> 1$. Thus equations (1) and (3) yield the following:

$$C_1^2 = \frac{5}{3}\frac{kT_1}{m_i} << u_1^2 \tag{6a}$$

$$V_{a_1}^2 = \frac{B_1^2}{m_i n_i \mu_0} << u_1^2 \tag{6b}$$

From satellite data it is known that the shock thickness is of the order of 10^4 meters and that it stands off from the magnetosphere a distance $\Delta \approx 0.3a$. There are several theoretical treatments of the bow shock structure (ref. 1, pp. 361 to 364). However, the shock thickness predicted by Tidman (refs. 3 and 4) shows the best agreement with satellite results. Tidman gives the shock thickness δ as

$$\delta = \frac{2\sqrt{\frac{kT_2}{m_2}}}{\frac{qB_1}{m_e}} \tag{7}$$

where δ is the order of the electron cyclotron radius, T_2 the temperature downstream of the shock, m_e the electron mass, and q the magnitude of the electron charge. Since the shock has a standoff distance $\Delta \sim 0.3a$ and $\Delta > \delta$, the shock thickness simulation criterion is

$$0.3a > \frac{2\sqrt{\frac{kT_2}{m_e}}}{\frac{qB_1}{m_e}} \tag{8}$$

GEOMETRY CRITERIA

From satellite data we know that $a = 10R_E$, where R_E is the radius of the Earth. Maintaining this geometrical similarity in a simulation experiment leads to a simulation criterion for the magnetic field. Using satellite information about the size of the interaction and also experimental data on the divergence angle of the MPD leads to a relation for the characteristic dimension of the experiment.

Several investigators have considered the shape of the boundary between a streaming plasma and a dipole field (i.e., the magnetosphere). These results are summarized in reference 1 (pp. 293 to 300). One of the results used to arrive at the simulation criterion is the following. The tangential magnetic field strength just inside the magnetopause is twice the strength of the field that would exist for an un-

disturbed dipole. For an undisturbed dipole the magnetic field along the Earth-Sun line is

$$B = B_E\left(\frac{R_E}{r}\right)^3 \tag{9}$$

where r is the distance from the center of the Earth and B_E is the magnetic field at the surface of the Earth. Therefore, for the case with flow, at the position a (fig. VII-3) the magnetic field is

$$B_a = 2B_E\left(\frac{R_E}{a}\right)^3 \tag{10}$$

Using the geometrical similarity result $a = 10R_E$ gives equation (10) as

$$B_a = 2\times10^{-3}\, B_E \tag{11}$$

It is more convenient to use the magnetic field strength on the axis of the dipole, which is denoted by B_P in figure VII-3. For a dipole, $B_P = 2B_E$. Therefore, equation (11) can be written as

$$B_a = 10^{-3}\, B_P \tag{12}$$

From satellite data it is known that the magnetosphere has a width of approximately 4a (fig. VII-3). Therefore, the plasma beam must satisfy the requirement

$$\text{Beam diameter} = d \geq 4a \tag{13}$$

Also, from experimental results it is known that the divergence angle of the MPD arc beam is approximately $\tan\theta \approx 1/4$ (fig. VII-3). Therefore, in order to satisfy the beam diameter requirement,

$$L \geq 8a \tag{14}$$

where L is the distance between the arc and the forward stagnation point located a distance a from the center of the dipole. A characteristic length for the experiment can now be established. Since the neutral sheet is to be investigated, it is necessary to maintain a collisionless flow downstream of the dipole. Based on satellite information, the distance $4a$ from the front of the magnetosphere is

chosen as a minimum distance for maintaining a collisionless flow. Therefore, referring to figure VII-2, the characteristic dimension of the experiment is

$$l \geq L + 4a = 12a \tag{15}$$

COLLISIONLESS CRITERIA

In the case of the solar wind, the only collisional mean free path to consider is the electron-ion. However, in a laboratory experiment where neutral atoms are present the electron-atom and ion-atom collisions must also be considered. For hydrogen, which is the gas most likely to be used in a simulation experiment, the electron-atom mean free path is larger than the other mean free paths. Therefore, if the restrictions on the electron-ion and ion-atom mean free paths are satisfied, the electron-atom mean free path is automatically larger than the dimensions of the experiment. First consider the electron-ion mean free path. If Spitzer's (ref. 6) deflection time t_D is used, the electron-ion mean free path is defined as follows:

$$\lambda_{ie} = u_1 t_D = \left(\frac{q^2}{4\pi\epsilon_0 m_i}\right)^{-2} \frac{u_1^4}{8\pi n_1 \ln \Lambda f(x)} \tag{16}$$

where ϵ_0 is the permittivity of free space. The function Λ is defined as

$$\Lambda = 1.55\times10^{13}\left(\frac{kT_1}{q}\right)^{3/2} n_1^{-1/2} \tag{17}$$

and since

$$x = u_1\left(\frac{2kT_1}{m_e}\right)^{-1/2} << 1 \tag{18}$$

the function f(x) can be approximated as

$$f(x) \approx \frac{4}{3\sqrt{\pi}} x \tag{19}$$

Substituting equation (19) into equation (16) yields the following simulation criterion:

$$l < \lambda_{ie} = 1.625\times10^{6}\, A_w^2 \left(\frac{kT_1}{q}\right)^{1/2} \frac{u_1^3}{n_1 \ln \Lambda} \tag{20}$$

where A_w is the atomic weight of the ion.

Now consider the ion-atom mean free path. Since the atom number density is controlled by the pumping rate of the vacuum facility, the ion-atom mean free path can be related to the pumping rate. If it is assumed that the plasma beam is fully ionized, then in steady-state operation the conservation of the heavy particles requires that

$$An_1u_1 = n_a\dot{V} \tag{21}$$

where A is the cross-sectional area of the beam, n_a the atom number density, and $\dot{V}$ the tank pumping speed. If the definition of the ion-atom mean free path

$$\lambda_{io} = \frac{1}{n_a\sigma_{io}} \tag{22}$$

is used, where σ_{io} is the ion-atom collision cross section, equation (21) yields the following simulation criterion:

$$l < \lambda_{io} = \frac{\dot{V}}{\sigma_{io}n_1u_1A} \tag{23}$$

There are several ion-atom cross sections (i.e., elastic and ionization). However, the largest of these is the charge-exchange cross section. Since λ_{io} is inversely proportional to σ_{io}, using the charge-exchange cross section is the most conservative way of requiring that $\lambda_{io} > l$. Values for σ_{io} as a function of ion velocity are given in reference 6.

DENSITY AND VELOCITY REQUIREMENTS

Table VII-1 lists the simulation criteria that must be satisfied. These conditions can all be expressed in terms of the upstream density n_1, the velocity u_1, and the parameter a.

If continuum one-dimensional flow expressions and the shock "jump" conditions are used, the shock thickness criteria can be reduced to an expression for n_1 as a function of a. The equation of motion for a one-dimensional plasma flow where the magnetic field is perpendicular to the flow direction is

$$m_i n u^2 + p + \frac{B^2}{2\mu_0} = \text{Constant} \tag{24}$$

This states that the sum of the momentum flux $m_i n u^2$, kinetic pressure p, and magnetic pressure $B^2/2\mu_0$ is a constant. At the stagnation point located at position a, $m_i n u^2 \to 0$ and $p \to 0$. Therefore, applying equation (24) to the flow along the stagnation line gives

$$m_i n_1 u_1^2 + p_1 + \frac{B_1^2}{2\mu_0} = m_i n_2 u_2^2 + p_2 + \frac{B_2^2}{2\mu_0} = \frac{B_a^2}{2\mu_0} \tag{25}$$

where the subscript 2 denotes conditions just downstream of the shock and subscript a denotes conditions at the stagnation point. The pressure is

$$p = nkT \tag{26}$$

Since both the acoustic Mach number and the Alfven number are much greater than 1 (eq. (6)), p and $B^2/2\mu_0$ can be neglected compared to $m_i n_1 u_1^2$. Therefore,

$$m_i n_1 u_1^2 \approx m_i n_2 u_2^2 + n_2 k T_2 + \frac{B_2^2}{2\mu_0} = \frac{B_a^2}{2\mu_0} \tag{27}$$

Also, for high Mach numbers the shock "jump" conditions of Tidman (refs. 3 and 4) are the following:

$$n_2 \approx 4 n_1 \tag{28a}$$

$$u_2 \approx \frac{1}{4} u_1 \tag{28b}$$

$$\frac{kT_2}{m_i} \approx \frac{3}{32} u_1^2 \tag{28c}$$

$$B_2 \approx 4B_1 \tag{28d}$$

Using equations (12) and (28) in equation (27) gives

$$B_P^2 = 2\mu_0 m_i n_1 u_1^2 \times 10^6 \tag{29}$$

and

$$B_1^2 = \frac{3}{64} \mu_0 m_i n_1 u_1^2 \tag{30}$$

If equations (28c) and (30) are now used in equation (8), the shock thickness criterion becomes

$$n_1 > \frac{25\times10^{14}}{a^2} m^{-3} \tag{31}$$

Equation (31) gives the minimum value of the density that satisfies the shock thickness criterion.

The mean free path requirements (eqs. (20) and (23)) can be reduced to relations between n_1 and u_1. First consider the electron-ion mean free path (eq. (20)). The high acoustic Mach number requirement sets the limit on T_1. For our purposes assume that $M_s \geq 4$. Therefore, from equation (1),

$$kT_1 \leq \frac{1}{16}\left(\frac{3}{5} m_i u_1^2\right) \tag{32}$$

Substituting equation (32) and $\ell = 12a$ into equation (20) yields

$$n_1 < \frac{10.7}{4 \ln \Lambda} A_w^{5/2} \frac{u_1^4}{a} \tag{33}$$

Now $\ln \Lambda$ is a slowly varying function of T_1 and n_1. For the densities and temperatures to be considered $\ln \Lambda \sim 10$. Therefore, for our purposes $(10.7/\ln \Lambda) \sim 1$, so that

$$n_1 < \frac{A_w^{5/2}}{4} \frac{u_1^4}{a} \tag{34}$$

Equation (34) determines the maximum density that will satisfy $\lambda_{ie} > \ell$.

The ion-atom mean free path requirement (eq. (23)) can be simplified by substituting $\ell = 12a$ and $A = 4\pi a^2$. Therefore, equation (23) gives

$$n_1 < \frac{1}{48\pi} \frac{\dot{V}}{a^3 \sigma_{io} u_1} \tag{35}$$

which sets another maximum limit on the number density.

Figure VII-4 shows the results obtained from equations (31) and (33) to (35) for $a = 0.2$. Results for two pumping speeds ($\dot{V}$) are shown. For $\dot{V} = 10^3$ cubic meters per second, which is the pumping speed of the present Lewis 15-foot-diameter vacuum tank, all the simulation requirements cannot be satisfied. However, at $\dot{V} = 5 \times 10^3$ cubic meters per second the shaded area in figure VII-4 is a region of u_1 and n_1 values that will satisfy all the requirements. Near-future modifications to the 15-foot vacuum tank should increase its pumping speed to 5×10^3 cubic meters per second to permit operation of an experiment in the shaded area of figure VII-4. The polar magnetic fields associated with these conditions are of the order of 1 tesla, which is a large field for a 4-centimeter-diameter magnet. If the value of a is increased, then the magnetic field requirement is reduced. At the same time, however, the region of acceptable u_1 and n_1 values is reduced. With a value of $a = 0.4$ meter there will still be a small range of acceptable velocities and densities for a pumping speed of $\dot{V} = 5 \times 10^3$ cubic meters per second. The polar magnetic field required will be of the order of 0.5 tesla. This size field should be no problem for an 8-centimeter-diameter magnet.

INITIAL EXPERIMENTAL RESULTS

As figure VII-4 shows, it is not possible to satisfy all the simulation criteria with the present experiment. However, conditions can be simulated for a collisionless stagnation flow. As a result, the initial investigation was in the stagnation region of the flow where a collisionless shock was expected to exist. Figure VII-5 shows the experiment in operation. The view is at an angle of approximately 45° from slightly behind the MPD arc. Measurements of the plasma potential and the magnetic field in the Z-direction were made in the region about half way between the thruster and the dipole (ref. 7). Table VII-2 compares the plasma properties of the

flow from the MPD arc with those of the solar wind. It is the ion-atom mean free path, which is approximately 1 meter, that limits the collisionless flow regime. This is the reason the investigation has been confined to the stagnation region close to the arc.

The first results obtained from the experiment indicated that the existence of a shock wave is unlikely. The Mach number of the flow is approximately 0.95. Since M_1 must be greater than 1 for a shock to form, it is concluded from these results that no shock can exist. Further evidence against the existence of a shock resulted from the plasma potential and magnetic field measurements.

The plasma potential V_p is shown in figure VII-6 as a function of distance from the dipole x. In figure VII-7, the magnetic field in the Z-direction B_z is presented as a function of x. To show where the magnetic field and plasma potential profiles are with respect to the light emitted, the results of figures VII-6 and VII-7 are superimposed on the results of figure VII-5. These results are shown in figure VII-8. Two different profiles of V_p appear in figure VII-6. The only major difference between the two is that the region of rapid increase moves back about 4 centimeters for the case where the dipole current is 495 amperes. This is as expected, since the stagnation magnetic field will be closer to the dipole for the lower current.

Both potential profiles show a rise of about 12 volts in the initial discontinuity. This rising potential region corresponds to a change in velocity given by

$$\frac{1}{2} m_i \left(u_1^2 - u_2^2\right) = q \, \Delta V_p \tag{36}$$

where ΔV_p is the change in potential, u_1 the upstream velocity, and u_2 the downstream velocity. If $\Delta V_p = 12$ volts and $u_1 = 5 \times 10^4$ meters per second, then for hydrogen ions equation (36) yields

$$u_2 = 4.5 \times 10^3 \text{ m/sec}$$

and

$$\frac{u_1}{u_2} = 11$$

The limiting velocity ratio for a shock is 4 (ref. 8). Therefore, this potential jump cannot represent a shock. However, it is very nearly the potential change that is required to stagnate hydrogen ions with a velocity of 5×10^4 meters per

second. To stagnate ions with $u_1 = 5\times10^4$ meters per second requires 13.1 volts.

Figure VII-7 shows that when the thruster is not operating the magnetic field has the usual $1/x^3$ dependence of a dipole field. When the thruster is operating, the magnetic field shows a change occurring in the same location as the rapid rise in the plasma potential. If the region of change is considered as lying between $x \sim 71$ and 59 centimeters, then

$$\frac{B_2}{B_1} \sim \frac{8\times10^{-4}}{3\times10^{-4}} = 2.7$$

If the change in magnetic field is assumed to occur across a shock, then from shock relations (ref. 8) this corresponds to $M_1 \sim 2.7$, which is higher than expected. Thus the magnitude of the magnetic field change also supports the contention that this region of change is not a shock.

When the measured plasma properties of equation (25) are used, the magnitude of the stagnation magnetic field can be calculated:

$$m_i n_1 u_1^2 + \frac{B_1^2}{2\mu_0} + n_1 k T_1 = \frac{B_a^2}{2\mu_0}$$

Using the values given in table VII-2 gives

$$B_a \sim 7\times10^{-4}\ \mathrm{T}$$

Referring to figure VII-7 shows that the 7×10^{-4} tesla point occurs at the end of the magnetic field change. This further substantiates the fact that the region of change in magnetic field and plasma potential is a stagnation flow rather than a shock wave. A more detailed study of the structure of the collisionless stagnation flow is certainly of interest. It may be useful in understanding the flow in the neighborhood of the magnetopause.

Besides investigating the stagnation region in our initial experiments, we have also visually observed regions of intense light in locations where we might expect to find radiation belts. However, no diagnostics of these regions have been made since in the present experiment some collisional processes are occurring.

FUTURE EXPERIMENTS

At the present time we are in the process of modifying the experiment to satisfy the simulation criteria previously outlined for the solar-wind - Earth interaction. The two things that must be done are to increase the pumping rate of the vacuum tank and to produce a higher Mach number flow. As has already been stated, the pumping rate of the vacuum tank is being increased to 5×10^3 cubic meters per second. This can be accomplished by adding a liquid helium cryopump to the tank. Two approaches are being investigated to produce a higher Mach number flow. First, the MPD arc will be modified to produce higher velocity flows. Second, the increased pumping rate will permit the dipole to be located further downstream. This should allow the thruster flow to expand to lower temperature and thus higher sonic Mach number. Once all the modifications are finished, a complete simulation may be possible.

REFERENCES

1. Hess, Wilmot N.: The Radiation Belt and Magnetosphere. Blaisdell Publishing Co., 1967.
2. Seikel, George R.; and Chubb, Donald L.: Simulation of Solar-Wind Magnetosphere Interactions. Bull. Am. Phys. Soc., series II, vol. 13, no. 7, July 1968, p. 959.
3. Tidman, D. A.: Turbulent Shock Waves in Plasmas. Physics of Fluids, vol. 10, no. 3, March 1967, pp. 547-564.
4. Tidman, D. A.: The Earth's Bow Shock Wave. J. Geophys. Res., vol. 72, no. 7, April 1, 1967, pp. 1799-1808.
5. Spitzer, Lyman: Physics of Fully Ionized Gases, 2nd edition, Wiley-Interscience Publishers, Inc., 1962.
6. McDaniel, Earl W.: Collision Phenomena in Ionized Gases, John Wiley & Sons, Inc., 1964, pp. 252-253.
7. Chubb, Donald L.: Laboratory Simulation of Solar Wind - Earth Interaction. NASA TM X-1738, 1969.
8. Ferraro, V. C. A.; and Plumpton, C.: An Introduction to Magneto-Fluid Mechanics. Oxford University Press, 1961, pp. 90-94.

TABLE VII-1. - SIMULATION CRITERIA

Simulation criteria	Analytical result
Shock thickness δ less than shock standoff distance $\Delta = 0.3a$	$0.3a > 2\sqrt{\frac{kT_2}{m_e}}\Big/\left(\frac{qB_1}{m_e}\right)$
Tangential magnetic field at magnetopause is twice the strength of field that would exist for an undisturbed dipole	$B_a = 10^{-3} B_p$
Electron-ion mean free path λ_{ie} greater than characteristic dimension of experiment $\ell = 12a$	$12a < 1.625\times10^6 A_w^2\left(\frac{kT_1}{q}\right)^{1/2} \frac{u_1^3}{n_1 \ln \Lambda}$
Ion-atom mean free path λ_{io} greater than characteristic dimension of experiment	$12a < \frac{\dot{V}}{\sigma_{io} n_1 u_1 A}$
Acoustic Mach number much greater than 1	$\frac{5}{3}\frac{kT_1}{q} << u_1^2$
Alfven number much greater than 1	$\frac{B_1^2}{m_i \mu_0 n_1} << u_1^2$

TABLE VII-2. - PROPERTIES OF PLASMA FLOW

Plasma property	Solar-wind experiment	Solar wind
Flow velocity, u_1, m/sec	5×10^4	4×10^5
Electron number density, n_1, cm^{-3}	2.6×10^{10}	3
Electron temperature, V	7	15
Upstream magnetic field, B_1, T	3×10^{-4}	4×10^{-9}
$\beta = n_1 kT_1 \Big/ \left(B_1^2/2\mu_0\right)$	0.8	1
Upstream acoustic Mach number, M_s	1.5	8
Upstream Alfven number, M_a	1.2	8
Electron-ion mean free path, m	10	10^5
Electron-neutral mean free path, m	10	---
Ion-neutral mean free path, m	1	---
Debye length, m	10^{-5}	10

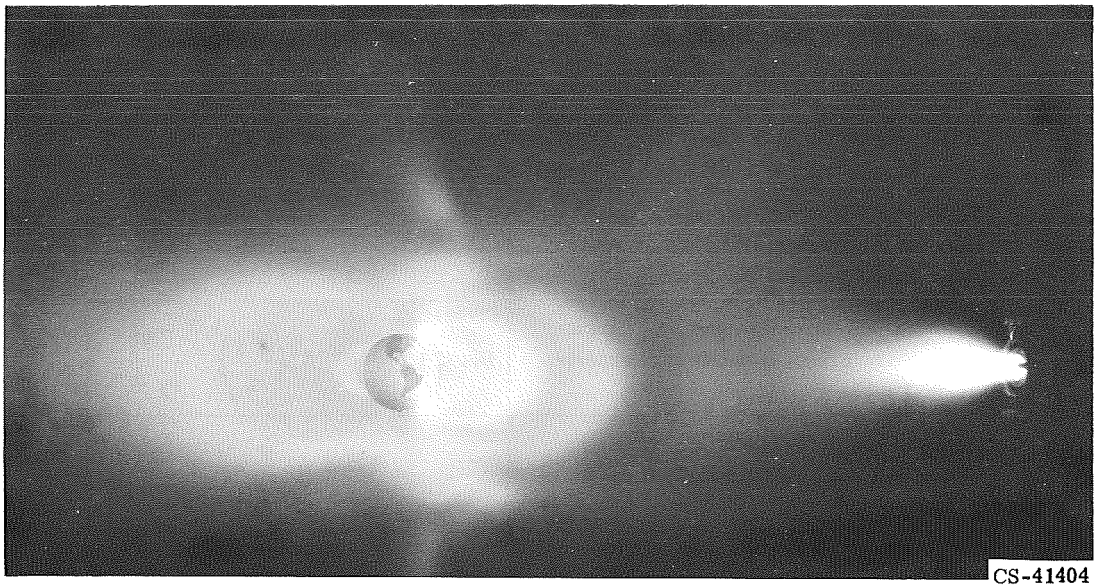

Figure VII-1. - Simulation experiment.

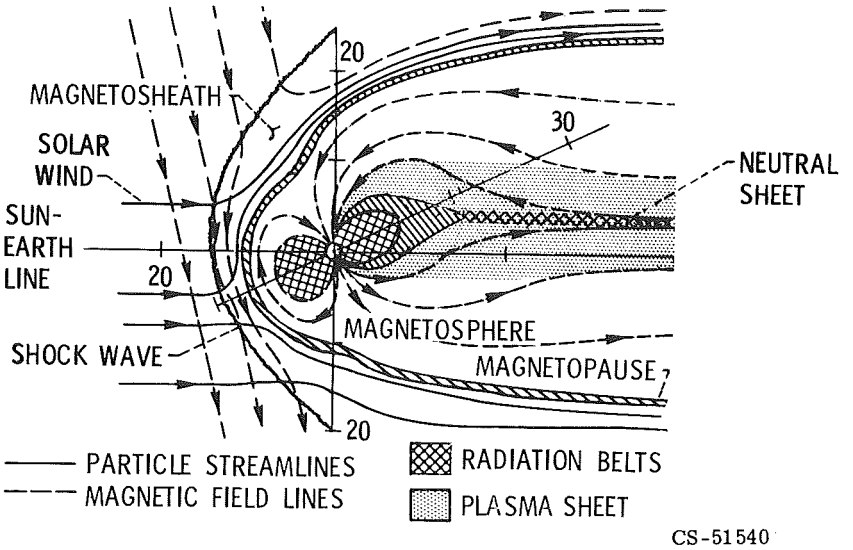

Figure VII-2. - Interaction of solar wind and Earth's field. Dimensionless distances are in terms of Earth radii, R_E.

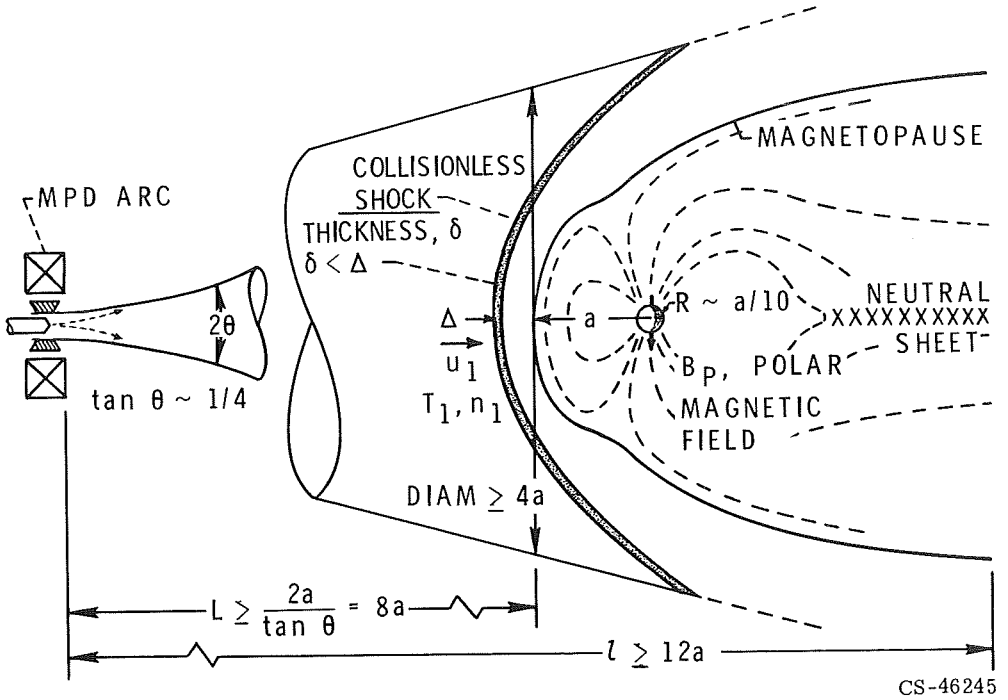

Figure VII-3. - Simulation of solar-wind - Earth interaction. Mean free paths $>> l$; $M_s >> 1$; $M_a >> 1$; $\delta < \Delta \sim 0.3$ a.

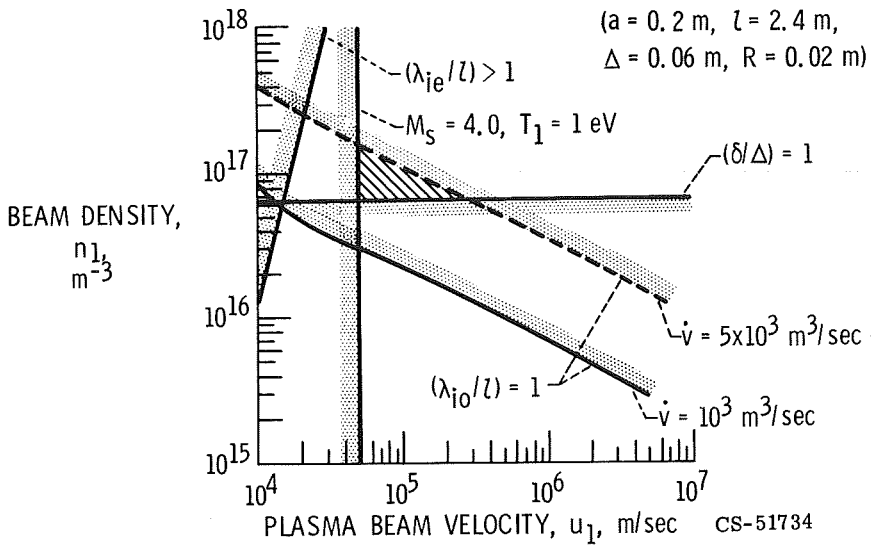

Figure VII-4. - Simulation criteria for stagnation point at 0.2 meter from magnet. (a = 0.2 m; l = 2.4 m; Δ = 0.06 m; R = 0.02 m.)

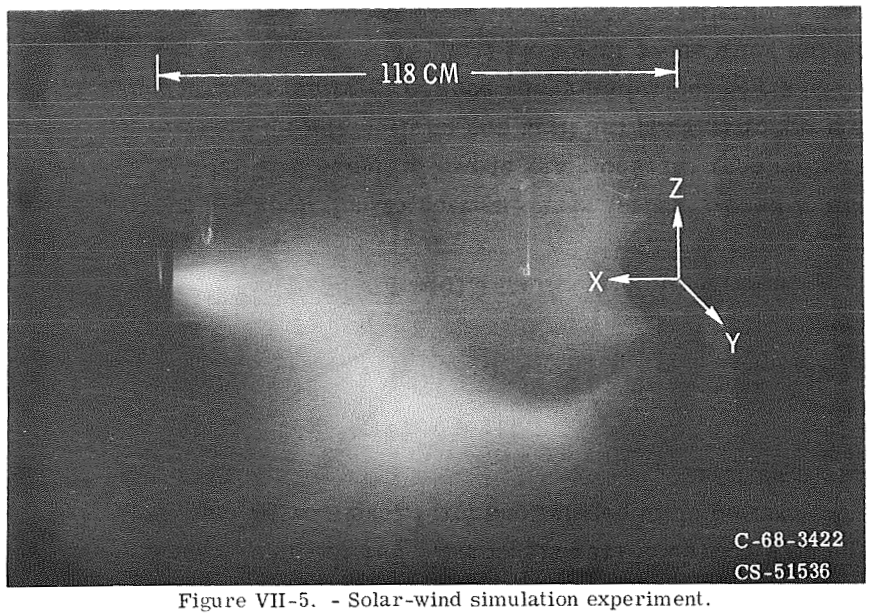

Figure VII-5. - Solar-wind simulation experiment.

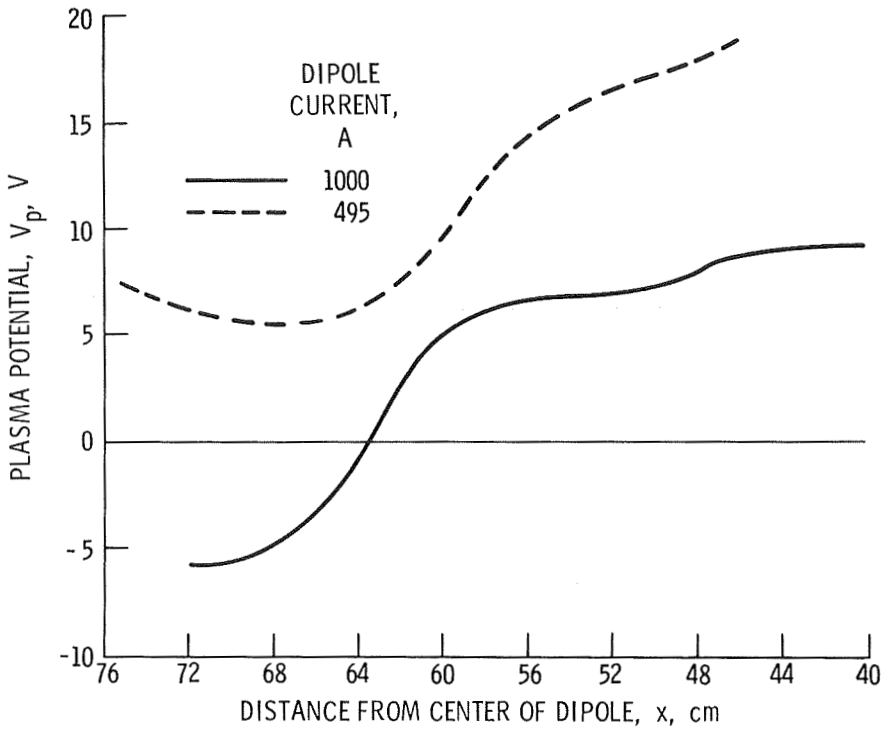

Figure VII-6. - Plasma potential profiles in stagnation region.

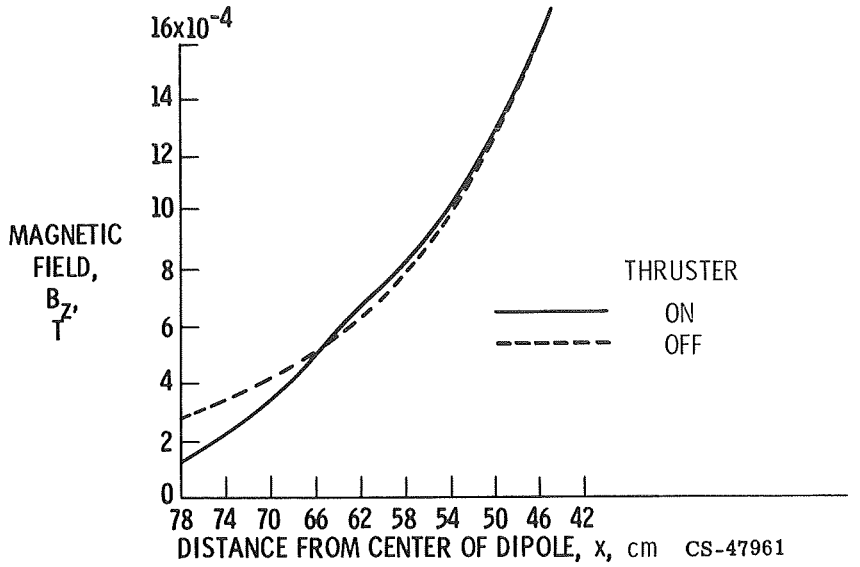

Figure VII-7. - Magnetic field profile in stagnation region. Dipole current, 1000 amperes.

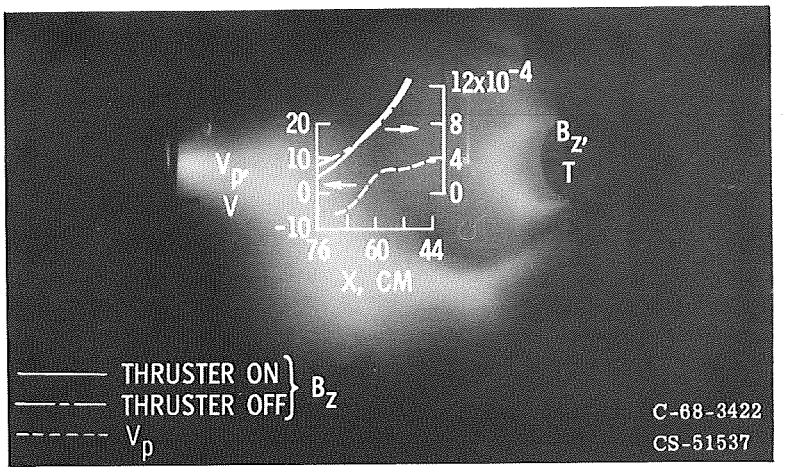

Figure VII-8. - Comparison of B_z and V_p profiles with emitted light.